Front. Earth Sci. 2018, 12(3): 506–520
https://doi.org/10.1007/s11707-018-0711-2

RESEARCH ARTICLE

Use of Sentinel-1 imagery for flood management in a reservoir-regulated river basin

T. PERROU (✉)[1], A. GARIOUD[2,3], I. PARCHARIDIS[1,2]

1 Department of Geography, Harokopio University of Athens, Athens, Greece
2 European Space Agency/ ESRIN, Frascati, Rome, Italy
3 Department of Geography, University Paris Diderot, Paris, France

Abstract Flood hazard monitoring and mapping is of great importance because it represents a significant contribution to risk management. The present study investigated the flood event that occurred downstream from the transboundary Strymon River basin, more specifically at Serres basin–a reservoir-regulated basin, in the beginning of 2015. The focus of this study was to better understand the spatio-temporal dynamic of the flood and the causes that initiated the hazard. Within the Serres basin, the Strymon transboundary river outflows to Lake Kerkini, which regulates water flow downstream for irrigation purposes and flood protection. For this research, a dataset of Sentinel-1 SAR GRD images was collected and processed covering the period of October 2014−October 2015 to investigate the water level changes in Lake Kerkini. Based on SAR images, binary water/non-water products and multitemporal RGB amplitude images were generated and interpreted. Sentinel-1 products have proved to be an effective tool on flood hazard dynamic extension mapping and estimation of water extent bodies retained by small reservoirs. In agreement with hydro-meteorological data and the high-resolution DEM, it was conceived that the flood event occurred due to the water volume flowing from upstream in the reservoir and the large amount of water draining from the tributaries into nearby sub-basins. Moreover, inefficient water management of the overwhelming water flow through the dam could further strengthen the flood event. The proposed approach, which is entirely based on open access remotely sensed data and processing tools, could be implemented in the same area for past flood events to produce archive retrospective data, as well as in other similar reservoir-regulated river basins in terms of water management and flood risk management.

Received July 17, 2017; accepted March 30, 2018

E-mail: dperrou@hua.gr, doraperrou@gmail.com

Keywords flood mapping, Sentinel-1, SAR, binary images, multitemporal image, river basin

1 Introduction

Both large and small reservoirs along rivers regulate downstream flows to generate hydropower. In many cases, they also store water for irrigation purposes and contribute to flood control during intensive rainfall periods. Failure in water management storage of artificial lakes can pose a hazard to people and infrastructures in downstream plains in terms of flooding. The potential flood hazard can have significant impacts, so it has to be monitored and assessed rapidly in order to mitigate impact and thus reduce the flood risk. Climate changes, due to anthropogenic impact in atmospheric composition, can intensify the global water cycle with a consequent increase in flood hazard and risk (Milly et al., 2002; Kundzewicz et al., 2014).

Reservoir management is critical, particularly for transboundary basins, where coordination between riparian countries is needed, but not always feasible. Such cases occur when water resources are shared between upstream and downstream countries (Crétaux et al., 2015). Several studies have been conducted in order to analyze flood cases in reservoir-regulated river basins (Peter et al., 2014; Motovilov et al., 2015; Albers et al., 2016; Gauvin et al., 2017; Sun and Xu, 2017; Vicente-Serrano et al., 2017) some of which have focused on the impacts of reservoir operation on flood inundation (Mateo et al., 2014; Ogilvie et al., 2016) or proposed responsibilities and regulations at a national level (Acford, 2015).

Satellite Earth Observations (EO) are a unique source of synoptic information that can supply regular, detailed updates on the status of hazards on a global, regional, or national basis. EO can simplify consistent and comparable implementation and monitoring and can link hazards, risk,

and climate. While obtaining suitable spatial and temporal resolution for observations is a challenge on a global basis, systems capable of monitoring the evolution of risk are in place (WCDRR, 2015).

EO satellite data are a complementary data source to in-situ and collateral data. When used jointly with *in-situ* data, they can provide an essential contribution for the creation of inventories of surface water resources to extract thematic maps relevant for hydrogeological studies and models (land cover, surface geology, lineaments, geomorphology) or for the retrieval of (bio)geophysical parameters (Schultz and Engman, 2000). Repeatability of observations allows the generation of time-series of the observed parameters and thereby achieving an improved capability to analyze, monitor, and forecast the evolution of the related phenomena, facilitating water resources management.

The most common approaches making use of EO for flood mapping are based on Synthetic Aperture Radar (SAR) data. Numerous studies from the past (Oberstadler et al., 1997; Pierdicca et al., 2013; Chini et al., 2016; Foumelis, 2017; Nakmuenwai et al., 2017) demonstrated that SAR satellite sensors are suitable tools for flood mapping. Flood extent mapping and dynamic monitoring is very important for the calibration and validation of hydraulic models (Horritt, 2006). It can also be used for damage assessment and risk management, and be a benefit to rescuers during flooding (Kussul et al., 2011).

The use of optical imagery for flood mapping is limited by severe weather conditions, particularly by the presence of clouds. Alternatively, SAR sensors are independent of the sun's electromagnetic radiation (EMR), emit their own microwave radiance, and record the amount of incident energy returned from the imaged surface (Klemas, 2015). SAR measurements offer valuable information for flood monitoring, regardless of weather conditions or time of day. Dependent on wavelength, SAR can penetrate emergent aquatic plants and forest canopies to detect the underlying standing water (Horritt et al., 2001; Brivio et al., 2002; Townsend, 2002; Lawrence et al., 2005), regardless of cloud cover. Parameters that affect and determine the response of the radar signal can be summarized by: (i) the system itself (direction of observation, frequency, wavelength, and polarization), (ii) the landscape characteristics and properties (roughness, moisture), and (iii) environmental and climatic factors (temperature, rain, fog, wind) (Curlander and McDonough, 1991).

One of the major advantages of using SAR images corresponds to the way the incoming microwave signal interacts with water. The ground, for its part, can influence the amount of radar return based on surface roughness, and generates a high contrast between ground and water surfaces. Smooth water bodies act as a mirror reflecting surface, the return backscatter signal towards the satellite is low or null, and thus water appears black in SAR imagery (Rees, 2001). At the same time, a wind-ruffled surface can give a strong backscatter signal larger than the surrounding land, and thus make it difficult to detect water surfaces on SAR images for flood applications.

Over the past decades, several studies have applied SAR data to map flood bodies using different techniques. Among the many flood extent mapping techniques currently available, commonly used methods are simple visual interpretation (Oberstadler et al., 1997), supervised classification (De Roo et al., 1999; Townsend, 2002), histogram thresholding (Hostache, 2006; Schumann et al., 2007), and several different multitemporal change detection methods (Bazi et al., 2005). Pierdicca et al. (2008) proposed a flood extraction algorithm considering both the SAR image and the Digital Elevation Model (DEM) of the region, so that waterlines (instantaneous land-water boundaries) in the outcome flood map were conditioned to vary in ground height along the river reach. Pulvirenti et al. (2011a) introduced a method that couples segmentation techniques and a SAR backscatter model. On a different note, the Schlaffer et al. (2012) study proposed harmonic analysis of a multitemporal ENVISAT Advanced SAR time series to delineate flood events. Additionally, it was found that the discrimination of inundated areas could be optimized by selecting the most suitable polarization of the radar waves. Henry et al. (2006) compared the ENVISAT ASAR with the performance of the SAR system on ERS-2 to evaluate the contribution of polarized configurations to flood boundary delineation.

The availability of the new EO products, such as Sentinel-1A & B imagery, have the potential to facilitate flood detection and monitoring of surface water changes which is dynamic in space and time (Bioresita et al., 2017). For the purpose of timely and effective operational services, a number of algorithms published in the relevant literature are available for producing flood extent maps in Near Real-Time (NRT) (Pulvirenti et al., 2011a; Chini et al., 2013) in addition to fully automated algorithms on demand (Martinis et al., 2015; Chini et al., 2017). Although much progress has been achieved in the development of NRT flood mapping procedures, the detection of inundation in complex environments, such as vegetated and urban areas, still requires further study (Chini et al., 2012; Giustarini et al., 2013; Pulvirenti et al., 2013, 2016). This is due to the fact that radar signatures of such targets are often ambiguous.

The dual-pol acquisition mode, the medium spatial resolution (20 m) with a very wide swath (250 km width), the high repeat cycle (temporal resolution of 6 days), and a relatively narrow orbit tube (small perpendicular baseline of interferometric acquisitions) of the Sentinel-1 mission are all characteristics that provide new momentum for the development of semi-automatic and automatic flood mapping algorithms.

This study focused on exploiting open access SAR data and open source software for image processing to increase

current knowledge on the flood hazards that occurred in a reservoir regulated river basin and in turn, contributed to risk prevention and mitigation.

The main objectives of the current research were to: (i) record the changes in water levels in an artificial reservoir and the spatio-temporal extent of the flood event that occurred downstream, and (ii) interpret EO-derived products with the hydro-meteorological data, and precipitation and water level measurements along the river to identify the potential causes that triggered the event.

In this study, SAR images from ESA's Sentinel-1 satellite were exploited to monitor the related water body extent changes in Lake Kerkini from October 2014 to October 2015, and at the same time, were used for dynamic flood hazard mapping downstream from the Transboundary Strymon River basin at the Serres basin (Fig. 1).

2 Study area

The Strymon/Struma River basin, has a total area of 16,747 km^2 and an approximate mean elevation of the catchment of 830 m. It is a transboundary basin shared by Bulgaria (50.6%, 8473 km^2), Greece (35.8%, 5990 km^2), FYROM (9.8%, 1641 km^2), and Serbia (3.8%, 643 km^2). It is fed by 58 tributaries of first and second order, 42 of which belong to the Bulgarian territory and 16 to the Greek territory. The total length of the river is about 390 km and springs from the Southern slopes of the Vitosha Mountain, in Bulgaria.

Sections of the transboundary Strymon River basin are located in Greece and in the northern region of central Macedonia, covering an area of 6472 km^2. Strymon River and Lake Kerkini are the chief surface water bodies in the basin, which in turn contribute ground water to the Serres basin.

Kerkini reservoir is commonly referred to as an artificial lake fed by the Strymon River which regulates water for irrigation purposes at the Serres Basin in addition to flood protection (Fig. 1). Maximum water volume in Lake Kerkini is 359.7×10^6 m^3 at a water level altitude of 36 m. (Doulgeris et al., 2008).

According to Vouvalidis (1994), the Strymon River, as well as the rest of the hydrographic network in the area, was formed during the second phase of the Graben evolution (Quaternary up to the beginning of the last century), while during the third phase (from the beginning of the last century), flood control prevention, drainage, and irrigation projects were conducted. This last period was characterized by the creation of a "man-made hydrography." Changes in bedding, and meander formation were also common.

The water level in the lake is controlled by the incoming flow of the Strymon River, which is controlled downstream through the Lithotopos dam. After the 1983

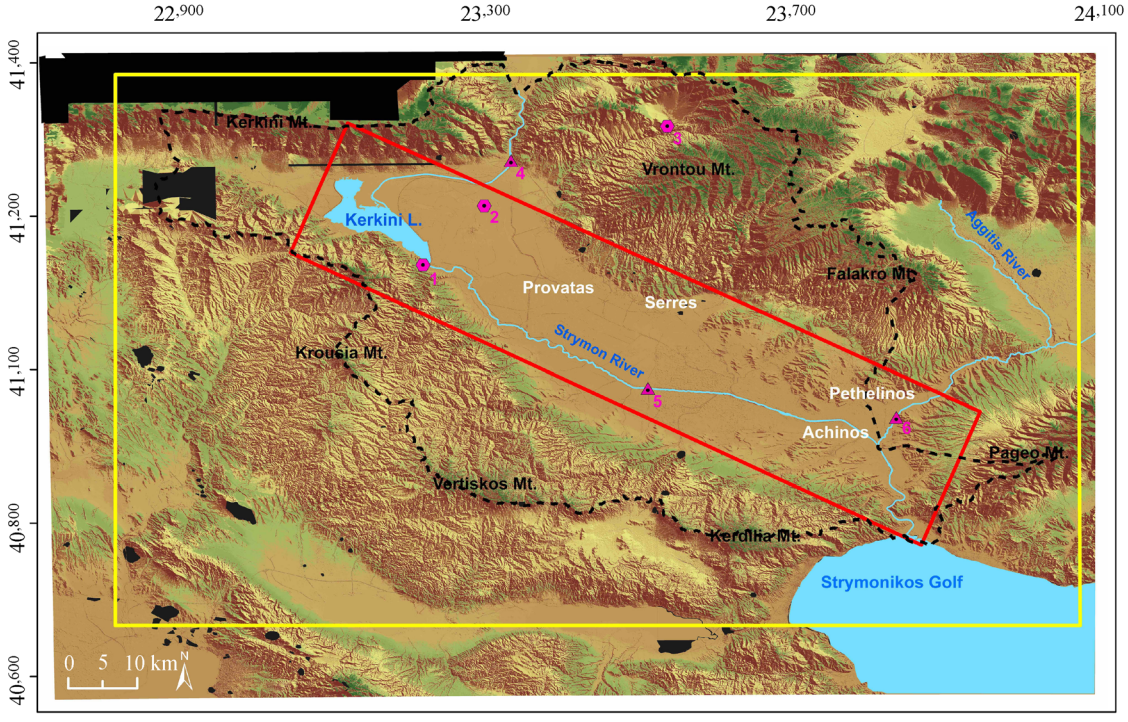

Fig. 1 Location map. SAR subset processed image (yellow frame), Serres basin (black dashed frame), area included in Figs. 4, 5, 6, and 7 (red frame), meteo-stations (polygons) 1: Lithotopos, 2: Koimissi Serron, 3: Achladochori, water level telemetry stations (polygons) 4: Trimeristis, 5: Nigrita, 6: Aggitis.

construction of the dam the lake was characterized by seasonal changes of approximately 5 m in the water level (Jerrentzup, 1992) which decreased potential flood risk. Another benefit was increased irrigation in the agricultural area of the lower Serres basin as excess runoff during rainy season is collected, providing greater water available during dry season. During the irrigation period (May to September), a maximum discharge of 40 m^3/s is released downstream from the lake, while a maximum amount of 200 m^3/s is released in Strymon River during the remainder of the year (Doulgeris et al., 2008). The efficient water resource management and use of the stored water in the reservoir has very positive socio-economic impacts on the livelihoods of the local inhabitants.

The dam affects the stratification conditions in the mouth of the Strymon River during spring and early summer (April to June) (Sylaios et al., 2010). In addition, the silting of the lake with debris from the Strymon River, and the deposition in the delta formed by the river at the entrance to Kerkini, creates a major problem by reducing the total volume of the water. The retention of sediment essentially reduces the effective water volume which in turn decreases the amount of water that can be stored, and may even defuse flood benefits.

The Serres basin, one of the most important sedimentary basins in northern Greece, is located in the southernmost part of an on-shore, intra-mountainous graben, part of the broader Strymon basin which is located in eastern Macedonia. Its area of 3.970 km^2 constitutes 23% of the total area of the catchment basin of Strymon. The basin is the final recipient of natural water throughout the Strymon's catchment located both within and outside Greece (Psilovikos et al., 1994). The present form of a river network within the Serres basin is primarily considered as natural, yet has been negatively impacted by human activities over the last few decades in the form of construction using hydraulics. The boundaries of the basin are defined by the following mountains: Kerkini (north) Kerdilia, Krousia, (west), and Falakro, Lekani, and Pageo (south-east).

The total thickness of the Neogene and Quaternary sediments at the center of the basin is approximately 4000 m (Syrides, 2000). The sediments found in the area of Achinos consist of basal conglomerates, limestone, sandstone, marl, silt, and clay with a total thickness ranging from a few meters to 1000 m (Karydakis et al., 2005).

Considering the Strymon River as a central axis, the basin presents an asymmetry relative to the height distribution, with the east-northeast at a higher elevation while the west-southwest is lower. The long axis measures 80 km at a NW/NE direction, while the small axis measures approximately 10 km with a NE/SW direction (Papafilipou-Pennou, 2004).

About 63% of the Serres basin is covered by marshes, lakes, ponds, and periodically by flooded land. Only 37% of the area was not threatened by floods. The large projects carried out in the area resulted in drainage of the ponds and marshes. The rehabilitation of several thousand acres were given to local population for cultivation. It is estimated that 62% of the previous lakes and stretches of land have been allocated for agricultural use. Among the improvement projects, including the drying of Achinos Lake, was the arrangement of the Strymon River bed and the remaking of the old Lake Kerkinitis, known today as Kerkini.

3 Data and methods

3.1 SAR dataset

Copernicus is an evolution of the Global Monitoring for Environment and Security program (GMES). This initiative, led by the European Commission (EC) in cooperation with the European Space Agency (ESA), is developing a new family of satellites called Sentinel. The Sentinels constitute the first series of operational satellites responding to the Earth observation needs of the European Union (EU) - ESA Global Monitoring for Environment and Security initiative (Torres et al., 2012). These satellites provide a unique set of observations starting with the all-weather radar images, day and night, from the Sentinel-1 A&B constellation. The Sentinel-1A, the first of the twin satellites, was launched in April 2014 by ESA, and was equipped with a C-band sensor, image swath of 250 km with the Interferometric Wide swath (IW) acquisition mode, spatial resolution of 5 m in range and 20 in azimuth, and a repeat time of 12 days. In April 2016, the Sentinel-1B was also placed successfully into orbit, decreasing the temporal resolution to 6 days.

The SAR sensor onboard the Sentinel satellite uses the Terrain Observation with Progressive Scans SAR (TOPSAR) mode to acquire images (De Zan and Monti Guarnieri, 2006).

Level 1 Ground Range Detected (GRD) Sentinel 1A C-band scenes were collected for this study from the Copernicus open Access Hub (https://scihub.copernicus.eu) on ESA's website. Level 1 GRD products concern SAR data detected, multi-looked, and projected to ground range using an earth Ellipsoid Model, with an approximate square pixel resolution.

A total number of 14 GRD SAR scenes, in descending and one in ascending Interferometric Wide (IW) swath mode, with polarization VV and VH, were collected spanning the period from October 2014 to October 2015 (Table 1). These data were processed and analyzed to create binary water/non-water products as well as SAR multitemporal products based on the contrast of the surface variations of land and water showing different backscattering signatures.

Table 1 Catalogue of Sentinel-1 SAR scenes used

Date	Orbit	Mode	Track/slice
2014/10/18	2879	Descending	7/5
2014/11/11	3229	Descending	7/5
2014/12/5	3579	Descending	7/5
2015/1/10	4104	Descending	7/5
2015/2/3	4454	Descending	7/5
2015/2/15	4629	Descending	7/5
2015/3/5	4899	Ascending	102/7
2015/3/11	4979	Descending	7/18
2015/4/16	5504	Descending	7/18
2015/5/22	6029	Descending	7/18
2015/6/27	6554	Descending	7/18
2015/7/21	6904	Descending	7/18
2015/8/26	7429	Descending	7/11
2015/9/7	7604	Descending	7/11
2015/10/25	8304	Descending	7/11

3.2 Climate & hydro-meteorological data

According to Papafilippou-Pennou (2004), the climate of the Serres basin, based on the investigation of meteorological data spanning the periods 1932–1940 and 1971–2002, can be characterized as Mediterranean, continental, and wet with hot-arid summer and marine type influences (transition type). In addition, based on the precipitation data under investigation, the author concluded that average monthly precipitation of all stations of the basin shows an annual rain trend with minimum and maximum values the first and last month of autumn, respectively. Numerous studies highlight the relationship between precipitation, which favors surface run-off in intense case, and river water level on floods in fluvial basins (Bullón, 2011; Sulaiman et al., 2017).

For the under-investigation period, the mean monthly accumulated precipitation from three meteorological stations (Fig. 2) was collected using the interactive map of the National Observatory of Athens/Institute of Environmental Research and Sustainable Development. We obtained data from the stations Achladochori (41.318°N/23.536°E), Lithotopos (41.137°N/23.217°E), and Koimissi Serron (41.214°N/23.297°E). As shown in Fig. 2, the rainfall was spread over the study period. The three meteorological stations showed the peak rainfall on December 2014 with an accumulated monthly amount of about 145 mm (Lithotopos Station). The second peak (100 mm for the three stations) appeared in March and the third in June (90 mm at Koimissi Serron Station), continuing the downward trend in rainfall rates.

Streamflow, which is the height of water in a stream related to the amount of water flow, is used in many ways, and is a crucial parameter concerning flood planning, management, and early warning systems (Herschy, 2009; Alfieri et al., 2013).

In this case study, only the parameter of the river water levels could be collected and used. Water level measurements were collected from a network of three different telemetry monitoring stations along the Strymon River provided by the Interbalkan Environment Center. The Trimeristis telemetry station (41.273245°N/23.331898°E) flow is near Trimeristis before Lake Kerkini, The Nigrita telemetry station (40.976333°N/23.510574°E) is located near the village Peponia, and the Aggitis telemetry station (40.938406°N/23.835413°E) is located at Aggitis River (Fig. 1).

Measurements were collected every fifteen minutes and then converted to a monthly average. In Fig. 2, the mean relative water level values are shown for the under-investigation period. The most significant change in water level observed in March and April 2015 at the Aggitis Station, where the water level increased (maximum 2 m), shows the trend water level apparently decreased. After April, there is a relative decrease of water level from the Aggitis Station and a slight increase from the Trimeristis Station.

3.3 Digital elevation products

A 3-arc-sec resolution Shuttle Radar Topography Mission (SRTM) v.4 DTM, from the Joint Research Center FTP, was automatically downloaded in tiles for the area covered by the SAR image with an approximate spatial resolution of 90 m/pixel.

The height information (EGM 96) was corrected to

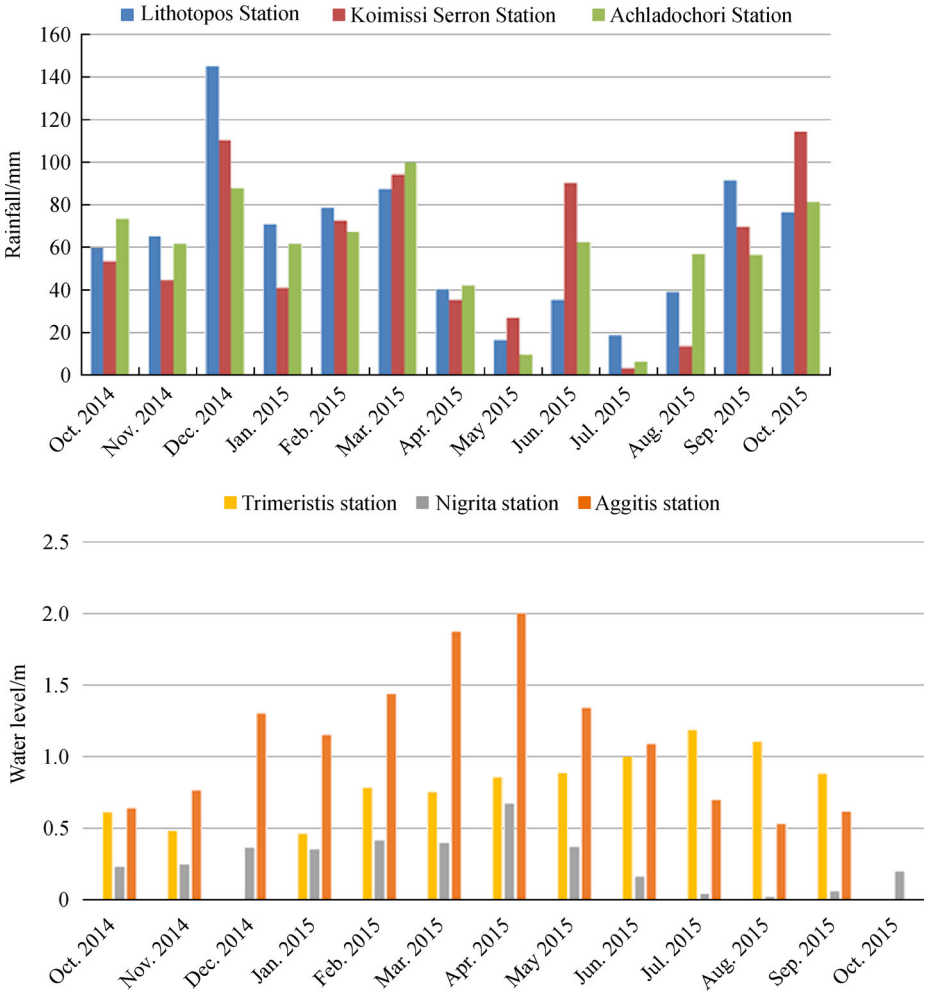

Fig. 2 Hydro-meteorological data. Precipitations (up) and water level changes (down) graphs.

obtain heights relative to the WGS84 ellipsoid. The DEM was used in the orthorectification step applying the Range-Doppler Terrain correction Method, and in synergy with other metadata, to derive the precise geolocation.

In addition, a Digital Elevation Model (DEM) in the WGS84 ellipsoid, with a very high resolution of 5 m/pixel and a vertical accuracy greater than 4 m, derived from airborne photogrammetry, provided by the National Cadastre and Mapping Agency SA of Greece, was used. This DEM was used to highlight the topography in the center of the Serres basin, and in particular, in the area of the old lake of Achinos.

4 SAR data processing

The pre-processing and main processing steps that were followed based on ESA's facilities (SNAP software version 5.0 and ESA's Virtual Machine RSS Cloud Toolbox), in addition to the other spatial data processing in terms of the validation process, are illustrated in Fig. 3.

Following orbit file refinement, a subset (Fig. 1) of the whole image was created by setting the values of the geographic coordinates per the following:

North latitude: 41.238°; west longitude: 24.073°; east longitude: 22.815°; south latitude: 40.814°.

After image subsetting, radiometric correction was applied so that pixel values could be directly related to radar backscatter. Image calibration is essential for quantitative use of the SAR data as the pixel values represent the true radar backscatter of the reflecting surface. This operation, among others, is necessary to produce multitemporal products. In the case of Sentinel-1 data, a calibration vector is included as an annotation allowing conversion of the image intensity values into sigma nought values (σ^0). From this step onward, the processing relates to the use of VV polarity.

The main problem associated with SAR data is speckle

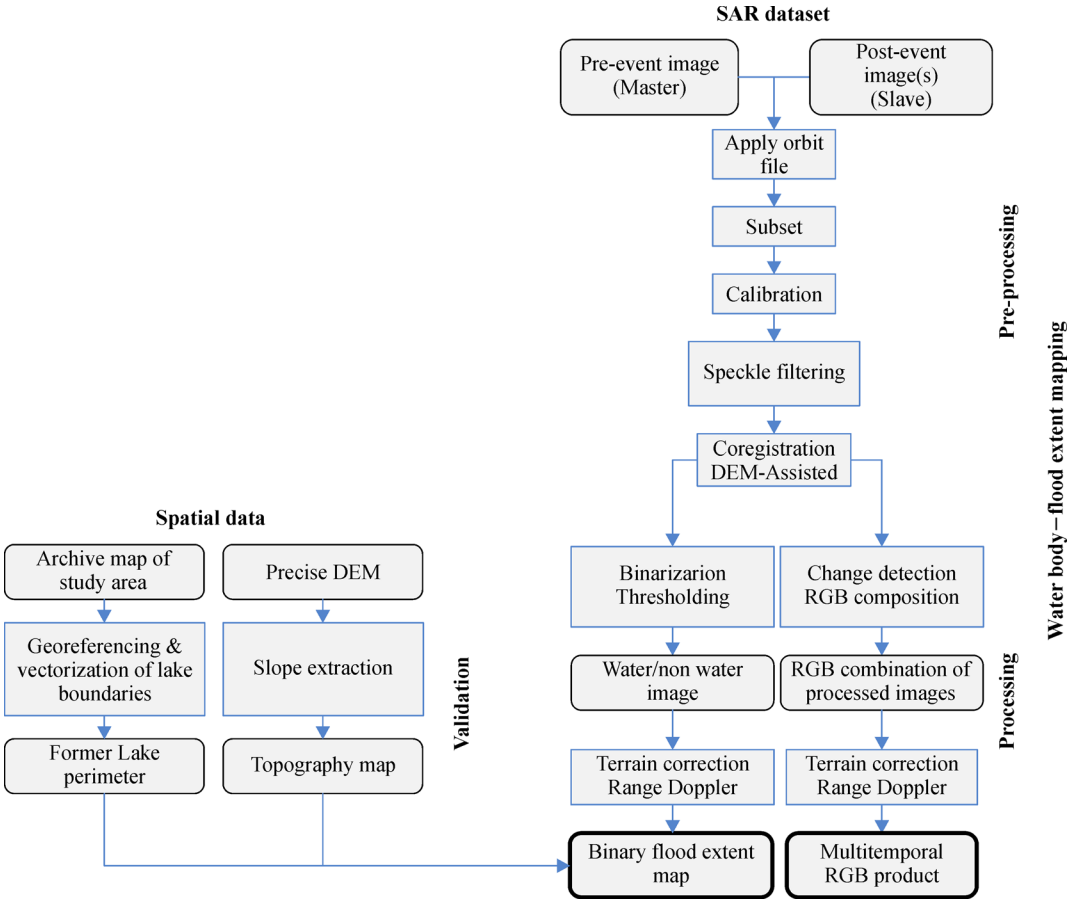

Fig. 3 Methodology flowchart. Water body- flood extent mapping methodology.

"noise" caused by the random effect of many small individual reflectors within a given pixel. In order to reduce the speckle, and at the same time preserve radiometric and textural information in SAR images to enhance the visualization, different adaptive filters were created. After comparison, the Gamma Map (Maximum a Posteriori) filter was applied using a kernel size of 5×5. The Gamma-Map filter assumes that the scene's reflectivity has a Gaussian distribution. Therefore, this filter uses a priori knowledge of the Probability Density Function (PDF) of the scene when suppressing the speckle of the scene (Nazry et al., 1991; Lopes et al., 1993).

The above-mentioned actions are considered as pre-processing steps. In this study, two products were generated based on SAR data: (i) binary images showing water and non-water areas over the study area, and (ii) multitemporal SAR images combining two or three dates to show spatio-temporal occurrence and seasonal evolution of the flood event.

For the water/non-water products generation, the image binarization technique was applied. The threshold segmentation algorithm or histogram thresholding is a simple but widely used and effective method to generate a binary image (Pulvirenti et al., 2011b). Similar methodology has been proposed in Perrou et al. (2017) for spatiotemporal flood mapping in a transboundary river basin. The first step to separate water from non-water areas through binarization is the calculation and selection of a suitable threshold for each image. For this purpose, the histogram of the filtered backscatter coefficient was investigated in a logarithmic scale in order to facilitate the process of selecting the threshold. Normally the histograms show two peaks (pixel value frequencies) of different magnitude of backscattering. Low values of the backscatter corresponded to the water, while high values corresponded to the non-water areas.

The aim was to specify the backscatter value separating the two sets of pixels. After numerous trials, the suitable threshold value was selected and applied in a band math expression to binarize every single SAR image in order to create water/non-water images showing the flooded areas and the permanent waters.

With the end of the in-orbit commissioning phase having been completed at the end of September 2014, Sentinel-1A data products were already consistently providing highly accurate geolocation (Schubert et al.,

2015). Since the obtained images were in the geometry of the sensor, it was necessary to re-project them into geographic projection.

The scenes were initially co-registered and stacked into a single reference (master) geometry. Given the spatial registration of the imagery is an essential requirement for effective change detection, the RMS value of the polynomial transformation of all pairs was decisively less than a pixel (0.05 of pixel). The Range Doppler orthorectification method (Small and Schubert, 2008) was used for geocoding the SAR images from 2D raster radar geometry, considering available information in the images' metadata about orbit state, radar timing annotation, and slant to ground range conversion parameters in combination with DEM (SRTM 3sec Arc) to derive precise geolocation information. The map projection type of the output images was expressed in WGS84 geographic coordinates.

5 Results

5.1 Water/non-water binary images

Based on the results of the binary water/non-water images, it was discerned that the first changes in the water's surface coverage was spotted in December 2014 when compared to October and November of the same year in Lake Kerkini and specifically in the area of the river delta of the lake. Water levels of the lake remained stable over December. There was a slight first indication of water coverage downstream from the basin along the river between the settlements of Achinos and Pethelinos in January 2015 (Fig. 4).

The first significant change in the shoreline of the lake, particularly in the north and east sections, occurred in February 2015. Downstream, near the area of Achinos-Pethelinos some water coverage was recorded southwards and specifically, immediately after the convergence of the Aggitis and Strymon Rivers. The Aggitis River drains a small basin to the west of the Serres basin (Fig. 4).

In the beginning of March 2015, while there was no significant change in the lake's water level, the flood phenomenon was ongoing both in the area of the old Achinos Lake and further south, immediately after the convergence with Aggitis (Fig. 4). In April, the lake's water level stabilized, while the phenomenon reached the maximum spatial coverage downstream, and the two flooded areas tended to join (Fig. 5).

In May 2015 (Fig. 5), there was a slight change in the lake's water level which actually decreased. The duration of the flood event was from March to July 2015. The most significant change was observed in the downstream where the southern inundated area drained, while in the area of old Lake Achinos, the standing water partially withdrew. During the dry period (June, July, August of 2015), the lake's water level continually decreased on the north and east coasts, with an accelerated water withdrawal from the flooded areas in the downstream. In September, when the lake's water level stabilized, no further indication of land under water was visible (Fig. 5).

5.2 Multitemporal images

Multitemporal SAR images have been increasingly used to detect different types of environmental changes (Ban and Hu, 2007; Inglada and Mercier, 2007; Balser and Wylie, 2010; Yousif and Ban, 2013). Surface characteristics that show change in SAR seasonal and interannual observations allow classification on the basis of temporal patterns. It has been demonstrated through several studies on various targets that color, multitemporal SAR data offer more information than single scenes (Kattenborn et al., 1993; Levsen et al., 1993). A methodology for temporary water body detection in semiarid environment is presented in Amitrano et al. (2017) based on multitemporal SAR data using COSMO-SkyMed stripmap.

In contrast to the main method of this research with single SAR image processing in terms of binarization, change detection through SAR multitemporal products highlight the temporal changes in land cover by comparing the flood scene to a previous dry image or the status of the flood within a time period.

To detect areas of backscatter changes, the processed SAR amplitude scenes were combined to generate multitemporal images in order to cover the seasonal-interannual evolution of the flood event in one image and to increase the temporal information.

The multitemporal image is the result of assigning intensity variations of three processed SAR images to each of the primary colors to form a Red Green Blue (RGB) image composition. Three Temporal Differentiate Images (TDI) were created (Fig. 6) after stacking each times three of the georeferenced images. Specifically, the following SAR images were combined: (i) images of 11 November 2014 (R) with 5 December 2014 (G) and 10 January 2015 (B) to show the pre-event phase, (ii) images of 3 February 2015 (R) with 11 March 2015 (G) and 16 April 2015 (B) to show the peak event period, and (iii) images of 22 May 2015 (R) with 27 June 2015 (G) and 21 July 2015 (B) to show the water withdrawal period. Finally, a two-date TDI image was created (Fig. 7) to show differences in water amounts in the Lake Kerkini between 18 October 2014 (R) and 25 October 2015 (G).

The color displayed in the generated multitemporal image is due to changes in the backscattering coefficients between the dates of acquisition of the three SAR images. Changes in the signal backscattering in this case could be attributed to changes provoked by land cover related phenomena or changes due to flood phenomenon evolution. The basin multicolors displayed in the multitemporal images are primarily produced by the different land-state

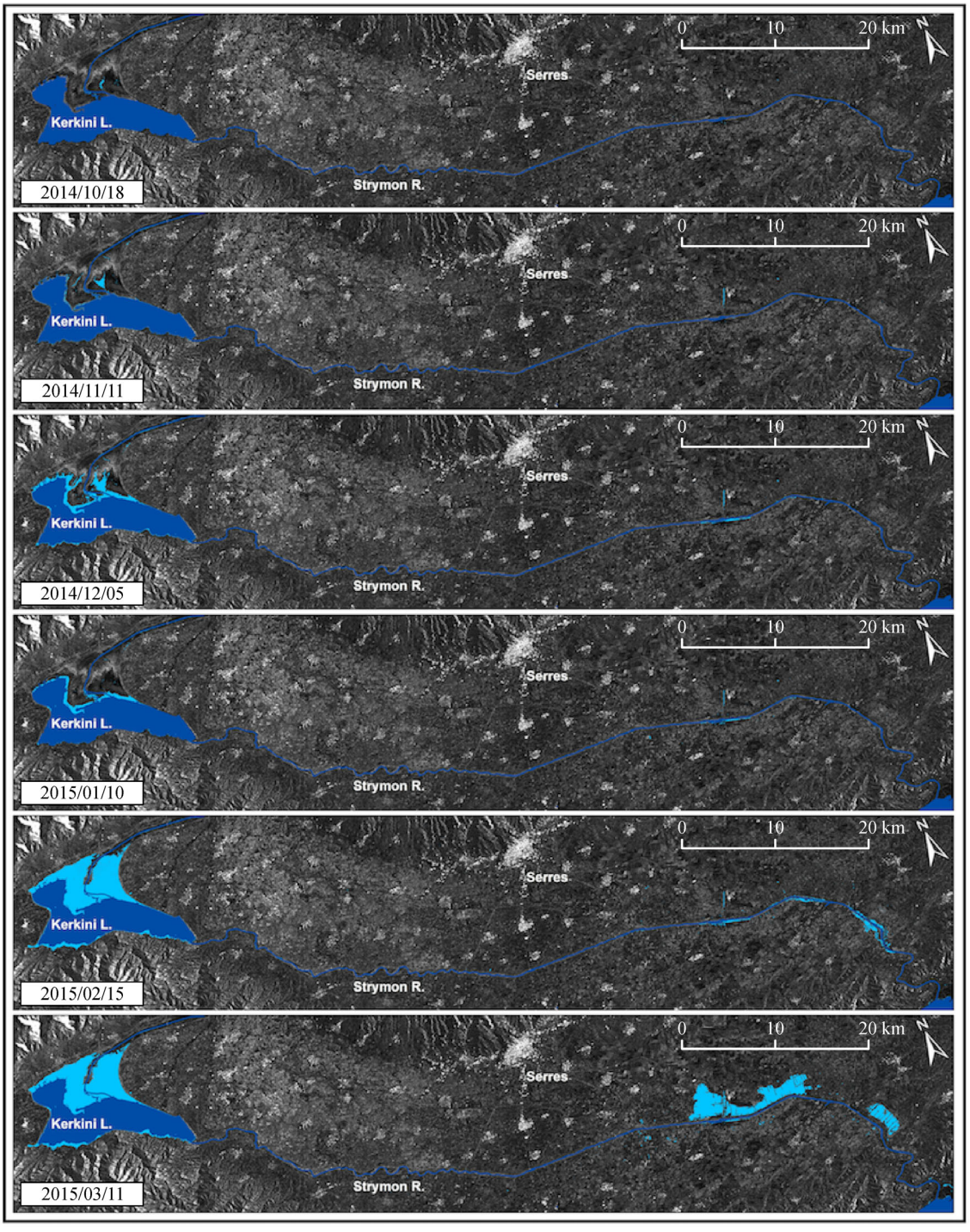

Fig. 4 Water/non-water. Binary images water/non-water from October 2014 to March 2015.

between the three acquisitions. The areas are shown in levels of white-grey-black where the land characteristics remain stable. The black and very dark grey shades on the images correspond to relatively constant, very low back-scattering surface features, such as the shadowed slopes, large roads, and drainage channels, and also areas under permanent or temporary water. The different colors are the result of the contribution of the backscatter intensity of an area for a particular date associated with an RGB color.

In the pre-event TDI, no significant changes could be distinguished in the outlet of Strymon River at Lake Kerkini, where the reddish colors correspond to the delta areas which, during December 2014 and January 2015, were covered by water due to the increased amount of

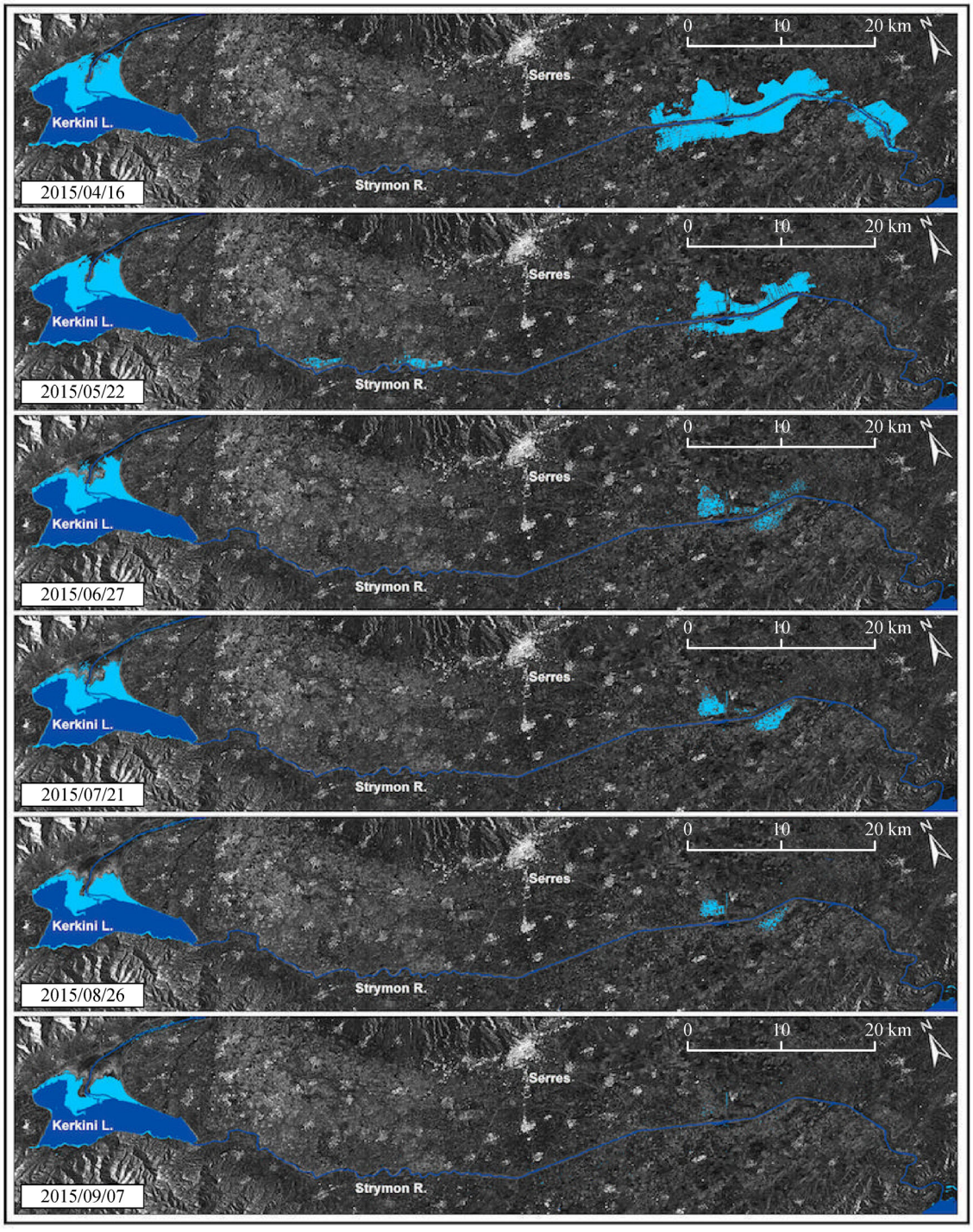

Fig. 5 Water/non-water. Binary images water/non-water from April 2015 to September 2015.

water. The mosaic of colors in the basin is related to changes due to crop development – white spots distributed in the basin correspond to the build-up areas confined to the area between Achinos and Pethelinos, and a red line indicates the beginning of the flood event. In the TDI covering the peak period (February-March-April), no significant changes were observed in the lake, but reddish colors were represented in the flooded areas downstream during March and April, and yellow colors appeared in the flooded areas in the image for April. The green colors in the basin are related to growth phases of the crops. In the TDI that corresponds to the dry period (May–June–July), no significant changes were identified in the lake, but there was a clear display change downstream where the flooded

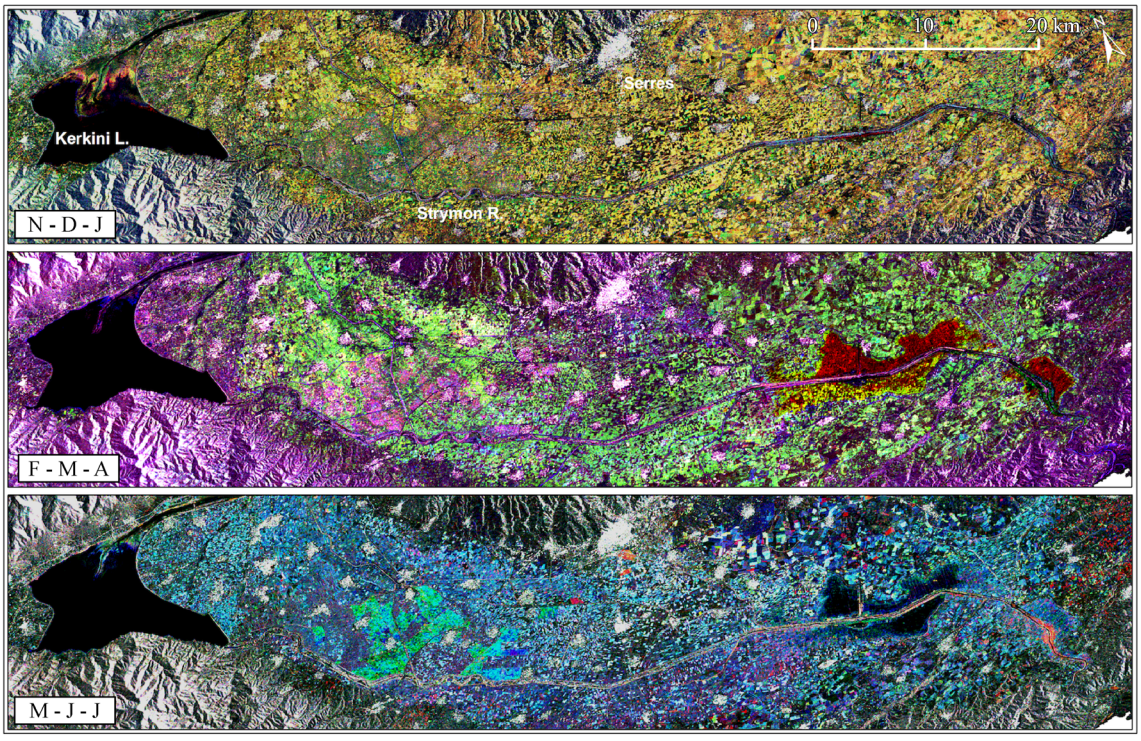

Fig. 6 Multitemporal. RGB, multitemporal SAR images, November (R)–December (G)–January (B) (up), February (R)–March (G)–April (B) (middle), May (R)–June (G)–July (B) (bottom).

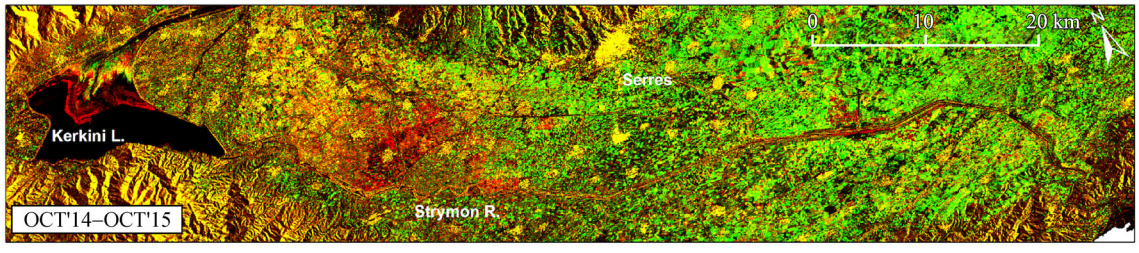

Fig. 7 Two-date SAR. A two-date multitemporal SAR image 18 October 2014 (R)–25 October 2015 (G) covering the Kerkini Lake downstream area.

areas next to the convergence of the rivers had drained in addition to a large section of the old Achinos Lake.

Finally, we deduce from the two-date TDI image from October 2014 to October 2015, and based on the dominance of reddish colors over the river delta in the northeast section of the lake that the amount of water appears to be significantly higher on the second date (Fig. 7).

6 Discussion and conclusions

The aim of the present study was to identify the causes that triggered the flood event by interpreting EO-derived flood mapping products in combination with *in-situ* hydro-meteorological data (precipitation, river water level measurements).

The main objective of the current research is to examine the EO flood application based on Sentinel-1 data for recording both changes in water levels in the Kerkini Lake reservoir from October 2014 to October 2015 and the dynamics of flood events that occurred at the beginning of 2015 downstream from the transboundary Strymon River at Serres basin. For both cases, flood extent retrospective products were created to improve flood-related knowledge for the study area. Sentinel-1 SAR imagery proved to be an effective tool by providing excellent spatiotemporal dynamic flood extent maps offering the possibility of processing the entire study area due to the extent of spatial coverage for each image. Mapping the variations in water

levels in the lake before, during, and after the flood event was also feasible with Sentinel-1 imagery.

The flood event occurred from March to July 2015, with the maximum flood extent taking place in April 2015 when the two flooded areas nearly merged to cover the entire area of the old Achinos Lake.

It was observed that there was a high correlation between the spatio-temporal characteristics of the event and the hydro-meteorological records for the under-investigated period.

The hypothesis stating that the flood event was primarily provoked by increased water flow into the lake from the Strymon River, in addition to the large amount of water that drained from the tributaries into other sub-basins nearby is supported in synergy with the hydro-meteorological and topography data. Indeed, the increase of water flow to the lake from upstream and the beginning of the flood event downstream occurred almost simultaneously.

Following the validation process, the hypothesis that the flood phenomenon occurred within the boundaries of the old Achinos Lake was confirmed. The vectorised boundaries of the old lake were almost identical to the boundaries of the maximum flood extent as illustrated in Fig. 8. Based on the results, the old Achinos Lake, including the area located immediately after its junction with Aggitis River (Fig. 8), are the most vulnerable due to the low topography and the presence of clayey-marly deposits which are impermeable and do not allow for ease of water flow.

Moreover, inefficient management of water release through the dam when water levels are high will likely intensify the likelihood for future flood events.

The significant contribution of the present study is the ability to identify the causes that could induce the flood phenomenon in a reservoir regulated river basin located downstream from a transboundary river basin, with space-based open access data and open source software. Lessons learned in terms of identifying the causes of a flood event are crucial and should be taken into consideration for future flood management in similar cases. The requirements revealed by this research are overall satisfied by Sentinel-1 A in terms of revisit, coverage, and systematic acquisition of free available data. Sentinel-1 B will further improve the results of the proposed research for future flood events. In addition, optical satellite data could be used as a complementary data source in such applications, dependent on weather conditions. Combining the different sensors (passive and active) information will allow for new possibilities in terms of temporal and spatial resolution.

The proposed methodology approach, based on open access data, ESA's open source software (SNAP), and semi-automatic algorithms, should also be applied for past events to create a repository database of retrospective flood extent maps contributing to a flood hazard assessment. The above-mentioned approach could be used as an effective operational tool by civil protection and local authorities to better understand the flood hazard in the area and to take appropriate measures and policies to prevent and/or to mitigate the impact.

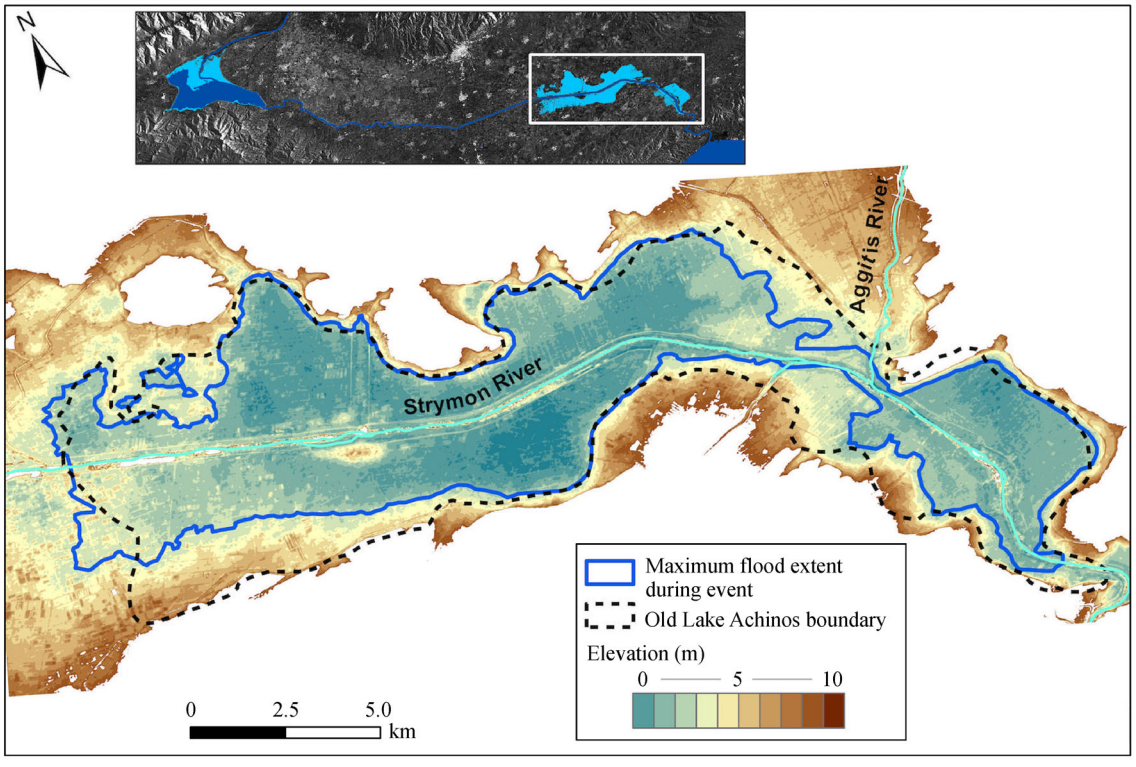

Fig. 8 Topography and inundation. Image showing relation between topography and maximum inundation in the area of the old Achinos Lake.

Finally, the current research approach can be repeated and applied to similar geomorphological environments of river basins controlled by a lake-reservoir to produce new results and increase current knowledge.

Acknowledgements Authors would like to thank the Lake Kerkini Management Authority, National Cadastre and Mapping Agency of Greece, and Serres basin Agricultural Cooperative. Authors would like to acknowledge the Interbalkan Environment Center for providing data in the framework of the River Alert project. Finally, the authors would like to thank the ESA Research and Service Support (RSS) team for supporting our processing work by providing a high performance Virtual Machine.

References

Acford M (2015). The reservoirs act 1975 and reservoir risk designations. Dams and Reservoirs, 25(2): 56–57

Albers S J, Déry S J, Petticrew E L (2016). Flooding in the Nechako River basin of Canada: a random forest modeling approach to flood analysis in a regulated reservoir system. Can Water Resour J, 41(1–2): 250–260

Alfieri L, Burek P, Dutra E, Krzeminski B, Muraro D, Thielen J, Pappenberger F (2013). GloFAS-global ensemble streamflow forecasting and flood early warning. Hydrol Earth Syst Sci, 17(3): 1161–1175

Amitrano D, Martino G D, Iodice A, Riccio D, Ruello G (2017). Small reservoirs extraction in semiarid regions using multitemporal synthetic aperture radar images. IEEE J Sel Top Appl Earth Obs Remote Sens, 10(8): 3482–3492

Balser A W, Wylie B K (2010). Multitemporal L- and C-band synthetic aperture radar to highlight differences in water status among boreal forest and wetland systems in the Yukon Flats, interior Alaska. U.S. Geological Survey Open-File Report 2010-1027, 18 p

Ban Y, Hu H (2007). Multitemporal RADARSAT-1 fine-beam SAR data for land-cover mapping and change detection. In: Proceedings Urban Remote Sens. Joint Event, Paris, France, 1–7

Bazi Y, Bruzzone L, Melgani F (2005). An unsupervised approach based on the generalized gaussian model to automatic change detection in multitemporal SAR images. IEEE Trans Geosci Remote Sens, 43(4): 874–887

Bioresita F, Puissant A, Stumpf A, Male J P (2017). Active and passive remote sensing data time series for flood detection and surface water mapping. Geophys Res Abstr, 19: EGU2017–10082

Brivio P A, Colombo R, Maggi M, Tomasoni R (2002). Integration of remote sensing data and GIS for accurate mapping of flooded areas. Int J Remote Sens, 23(3): 429–441

Bullón T (2011). Relationships between precipitation and floods in the fluvial basins of Central Spain based on documentary sources from the end of the 16th century. Nat Hazards Earth Syst Sci, 11(8): 2215–2225

Chini M, Hostache R, Giustarini L, Matgen P (2017). A hierarchical split-based approach for parametric thresholding of SAR images: flood inundation as a test case. IEEE Trans Geosci Remote Sens, 55 (12): 6975–6988

Chini M, Papastergios A, Pulvirenti L, Pierdicca N, Matgen P, Parcharidis I (2016). SAR coherence and polarimetric information for improving flood mapping. In: Proceedings of the International Geoscience and Remote Sensing Symposium (IGARSS), Beijing, China, 10−15 July, 2016, 7577–7580

Chini M, Piscini A, Cinti F R, Amici S, Nappi R, De Martini P M (2013). The 2011 Tohoku-Oki (Japan) tsunami inundation and liquefaction investigated by optical, thermal and SAR data. IEEE Geosci Remote Sens Lett, 10(2): 347–351

Chini M, Pulvirenti L, Pierdicca N (2012). Analysis and interpretation of the COSMO-SkyMed observations of the 2011 Japan Tsunami. IEEE Geosci Remote Sens Lett, 9(3): 467–471

Curlander J C, McDonough R N (1991). Synthetic Aperture Radar: Systems and Signal Processing. New York: John Wiley and Sons

De Roo A J, Van Der Knijff M, Horritt G, Schmuck De Jong S (1999). Assessing flood damages of the 1997 Oder flood and the 1995 Meuse flood. Paper presented at 2nd International ITC Symposium on Operationalization of Remote Sensing, Enschede, Netherlands

De Zan F, Monti Guarnieri A M (2006). TOPSAR: terrain observation by progressive scans. IEEE Trans Geosci Remote Sens, 44(9): 2352–2360

Doulgeris Ch, Halkidis I, Papadimos D (2008). Use of modern technology for the protection and management of water resources in Strymonas/Struma River basin. The Goulandris Natural History Museum- Greek Biotope/Wetland Centre. Thermi, Greece. p. 82

Foumelis M (2017). Impact of dam failure induced flood on road network using combined remote sensing and geospatial approach. J Appl Remote Sens, 11(1): 016004

Gauvin C, Delage E, Gendreau M (2017). Decision rule approximations for the risk averse reservoir management problem. Eur J Oper Res, 261(1): 317–336

Giustarini L, Hostache R, Matgen P, Schumann G J P, Bates P D, Mason D C (2013). A change detection approach to flood mapping in urban areas using TerraSAR-X. IEEE Trans Geosci Remote Sens, 51(4): 2417–2430

Henry J B, Chastanet P, Fellah K, Desnos Y L (2006). ENVISAT multi-polarised ASAR data for flood mapping. Int J Remote Sens, 27(10): 1921–1929

Herschy R W (2009). Streamflow Management. Rouledge publisher, London, p. 507

Horritt M S (2006). A methodology for the validation of uncertain flood inundation models. J Hydrol (Amst), 326(1–4): 153–165

Horritt M S, Mason D C, Luckman A J (2001). Flood boundary delineation from synthetic aperture radar imagery using a statistical active contour model. Int J Remote Sens, 22(13): 2489–2507

Hostache R (2006). Satellite image analysis for three-dimensional flood hazard characterisation and hydrolic modelling support. Dissertation for PhD degree. Sciences of the Universe, UMR Territories, Environment, Remote Sensing and Spatial Information, Cemagref/ ENGREF/CIRAD, Montpellier, France, p. 197 (in French)

Inglada J, Mercier G (2007). A new statistical similarity measure for change detection in multitemporal SAR images and its extension to multiscale change analysis. IEEE Trans Geosci Remote Sens, 45(5): 1432–1445

Jerrentzup H (1992). The fauna of Lake Kerkini. In: Gerakis P A, ed. Conservation and Management of Greek Wetlands. Proceedings of a Greek Wetlands Workshop, Thessaloniki, Greece, 1989, IUCN, Gland, Switzerland

Karydakis A, Arvanitis A, Andritsos N, Fytikas M (2005). Low enthalpy geothermal fields in the Strymon Basin (Northern Greece). In: Proceedings World Geothermal Congress 2005 Antalya, Turkey, 24–29 April, 2005

Kattenborn G, Nezry E, De Grandi G, Sieber A J (1993). High resolution detection and monitoring of changes using ERS-1 time series. In: Proceedings of 2nd ERS-1 Symposium, Hamburg, Germany, 11–14 October, 1993 (ESA, ESTEC: The Netherlands). 635–642

Kiage L M, Walker N D, Balasubramanian S, Babin A, Barras J (2005). Applications of Radarsat-1 synthetic aperture radar imagery to assess hurricane-related flooding of coastal Louisiana. Int J Remote Sens, 26 (24): 5359–5380

Klemas V (2015). Remote sensing of floods and flood-prone areas: an overview. J Coast Res, 31(4): 1005–1013

Kundzewicz Z W, Kanae S, Seneviratne S I, Handmer J, Nicholls N, Peduzzi P, Mechler R, Bouwer L M, Arnell N, Mach K, Muir-Wood R, Brakenridge G R, Kron W, Benito G, Honda Y, Takahashi K, Sherstyukov B (2014). Flood risk and climate change: global and regional perspectives. Hydrol Sci J, 59(1): 1–28

Kussul N, Shelestov A, Skakun S V (2011). Flood Monitoring from SAR Data. In: Kogan F, Powell A, Fedorov O, eds. Use of Satellite and In-situ Data to Improve Sustainability. NATO Science for Peace and Security Series C: Environmental Security. Springer: 19–29

Levsen M, Conway J A, Sieber A (1993). Evaluating multitemporal ERS-1 data for tropical forest mapping: regional mapping and change detection applications. In: Proceedings of 2nd ERS-1 Symposium, Hamburg, Germany, 11–14 October, 1993 (ESA, ESTEC: The Netherlands)

Lopes A, Nezry E, Touzi R, Laur H (1993). Structure detection and statistical adaptive speckle filtering in SAR images. Int J Remote Sens, 14(9): 1735–1758

Martinis S, Kersten J, Twele A (2015). A fully automated TerraSAR-X based flood service. ISPRS J Photogramm Remote Sens, 104: 203–212

Mateo C M, Hanasaki N, Komori D, Tanaka K, Kiguchi M, Champathong A, Sukhapunnaphan T, Yamazaki D, Oki T (2014). Assessing the impacts of reservoir operation to floodplain inundation by combining hydrological, reservoir management, and hydrodynamic models. Water Resour Res, 50(9): 7245–7266

Milly P C D, Wetherald R T, Dunne K A, Delworth T L (2002). Increasing risk of great floods in a changing climate. Nature, 415 (6871): 514–517

Motovilov Y, Danilov-Danilyan V, Dod E, Kalugin A (2015). Flood protection effect of the existing and projected reservoirs in the Amur River basin: evaluation by the hydrological modelling system. In: the IAHS-AISH Proceedings and Reports, 370: 63–67

Nakmuenwai P, Yamazaki F, Liu W (2017). Automated extraction of inundated areas from multitemporal dual-polarization radarsat-2 images of the 2011 central Thailand flood. Remote Sens, 9(1): 78

Nazry E, Lopes A, Touzi R (1991). Detection of structural and textural features for SAR images filtering. Proceedings of IGARSS, 91: 2169–2172

Oberstadler R, Hönsch H, Huth D (1997). Assessment of the mapping capabilities of ERS-1 SAR data for flood mapping: a case study in Germany. Hydrol Processes, 11(10): 1415–1425

Ogilvie A, Belaud G, Massuel S, Mulligan M, Le Goulven P, Calvez R (2016). Assessing floods and droughts in ungauged small reservoirs with long-term landsat imagery. Geosciences (Switzerland), 6(4), https://doi.org/10.3390/geosciences 6040042

Papafilippou-Pennou E (2004). Dynamic Evolution and Recent Exogenic Processes of (Strymon) River Network in Serres Graben (North Greece). Dissertation for PhD degree. Department of Physical Environmental Geography, School of Geology, Faculty of Sciences, Aristotle University of Thessaloniki. 1–243

Perrou T, Papastergios A, Parcharidis I, Chini M (2017). Spatiotemporal hazard mapping of a flood event 'migration' in a Transboundary River Basin as an operational tool in Flood Risk Management. In: Proceedings of SPIE 10426, Active and Passive Microwave Remote Sensing for Environmental Monitoring, 104260A (3 October 2017)

Peter S J, De Araújo J C, Araújo N A M, Herrmann H J (2014). Flood avalanches in a semiarid basin with a dense reservoir network. J Hydrol (Amst), 512: 408–420

Petiteville I, Ward S, Dyke G, Steventon M, Harry J (2015). Satellite Earth Observations in Support of Disaster Risk Reduction. CEOS Earth Observation Handbook, 3rd UN World Conference on Disaster Risk Reduction: European Space Agency

Pierdicca N, Chini M, Pulvirenti L, Macina F (2008). Integrating physical and topographic information into a fuzzy scheme to map flooded area by SAR. Sensors (Basel), 8(7): 4151–4164

Pierdicca N, Pulvirenti L, Chini M, Guerriero L, Candela L (2013). Observing floods from space: experience gained from COSMO-SkyMed observations. Acta Astronaut, 84: 122–133

Psilovikos A, Papafilippou-Pennou E, Albanakis K, Vouvalidis K (1994). Bedload transport and deposition in the river Strymon artificial channel before its reach to the Kerkini reservoir. Bulletin of Geological Society of Greece, XXX(4): 149–155

Pulvirenti L, Chini M, Pierdicca N, Boni G (2016). Use of SAR data for detecting floodwater in urban and agricultural areas: the role of the interferometric coherence. IEEE Trans Geosci Remote Sens, 54(3): 1532–1544

Pulvirenti L, Chini M, Pierdicca N, Guerriero L, Ferrazzoli P (2011b). Flood monitoring using multitemporal COSMO-SkyMed data: image segmentation and signature interpretation. Remote Sens Environ, 115 (4): 990–1002

Pulvirenti L, Pierdicca N, Chini M, Guerriero L (2011a). An algorithm for operational flood mapping from synthetic aperture radar (SAR) data using fuzzy logic. Nat Hazards Earth Syst Sci, 11(2): 529–540

Pulvirenti L, Pierdicca N, Chini M, Guerriero L (2013). Monitoring flood evolution in vegetated areas using COSMOSkyMed data: the Tuscany 2009 case study. IEEE J Sel Top Appl Earth Obs Remote Sens, 6(4): 1807–1816

Rees W G (2001). Physical Principles of Remote Sensing. Cambridge University Press

Schlaffer S, Hollaus M, Wagner W, Matgen P (2012). Flood delineation from synthetic aperture radar data with the help of a priori knowledge from historical acquisitions and digital elevation models in support of near-real-time flood mapping. In: Proceedings of SPIE- the International Society for Optical Engineering, 8538

Schubert A, Small D, Miranda N, Geudtner D, Meier E (2015). Sentinel-1A product geolocation accuracy: commissioning phase results.

Remote Sens, 7(7): 9431–9449

Schultz G A, Engman E T (2000). Remote Sensing in Hydrology and Water Management. Berlin: Springer-Verlag

Schumann G, Hostache R, Puech C, Hoffmann L, Matgen P, Pappenberger F, Pfister L (2007). High-resolution 3D flood information from radar for effective flood hazard management. IEEE Trans Geosci Remote Sens, 45(6): 1715–1725

Small D, Schubert A (2008). A guide to ASAR geocoding, RSL-ASAR-GC-AD, Issue 1.0. University of Zurich

Sulaiman N H, Kamarudin M K A, Toriman M E, Juahir H, Ata F M, Azid A, Wahab N J A, Umar R, Khalit S I, Makhtar M, Arfan A, Sideng U (2017). Relationship of rainfall distribution and water level on major flood 2014 in Pahang River Basin, Malaysia. Environ Asia, 10(1): 1–8

Sun X, Xu M (2017). Optimal control of water flooding reservoir using proper orthogonal decomposition. J Comput Appl Math, 320: 120–137

Sylaios G K, Kamidis N, Tsihrintzis V A (2010). Impact of river damming on coastal stratification–mixing processes: the cases of Strymon and Nestos Rivers, N. Greece. Desalination, 250(1): 302–312

Syrides G (2000). Neogene marine cycles in Strymon basin, Macedonia, Greece. Geological Society of Greece, Special Publications in: Proceedings Interim Colloquim RCMNS, Patras, Greece, May 1988, 217–225

Torres R, Snoeij P, Geudtner D, Bibby D, Davidson M, Attema E, Potin P, Rommen B, Floury N, Brown M, Navas Traver I, Deghaye P, Duesmann B, Rosich B, Miranda N, Bruno C, L'Abbate M, Croci R, Pietropaolo A, Huchler M, Rostan F (2012). GMES Sentinel-1 mission. Remote Sens Environ, 120: 9–24

Townsend P A (2002). Relationships between forest structure and the detection of flood inundation in forested wetlands using C-band SAR. Int J Remote Sens, 23(3): 443–460

Vicente-Serrano S M, Zabalza-Martínez J, Borràs G, López-Moreno J I, Pla E, Pascual D, Savé R, Biel C, Funes I, Azorin-Molina C, Sanchez-Lorenzo A, Martín-Hernández N, Peña-Gallardo M, Alonso-González E, Tomas-Burguera M, El Kenawy A (2017). Extreme hydrological events and the influence of reservoirs in a highly regulated river basin of northeastern Spain. Journal of Hydrology: Regional Studies, 12: 13–32

Vouvalidis K (1994). Natural and anthropogenic processes that contribute to the development of the river Strymon estuary, N. Greece. Dissertation for PhD degree. Aristotle University of Thessaloniki, Faculty of Sciences, School of Geology, Department of Physical Environmental Geography, p. 192

Yousif O, Ban Y (2013). Improving urban change detection from multitemporal SAR images using PCA-NLM. IEEE Trans Geosci Remote Sens, 51(4): 2032–2041